EasyChair Preprint

№ 7667

Void Growth Based Damage Model for the Anisotropic Material

Hao H. Nguyen and Hoa C. Vu

March 29, 2022

Void Growth Based Damage Model for the Anisotropic material

Hao H. Nguyen[1] and Hoa C. Vu[1]

[1] Department of Engineering Mechanics, Ho Chi Minh City University of Technology (HCMUT) – VNU-HCM, Ho Chi Minh City, Viet Nam
nguyenhuuhao@hcmut.edu.vn

Abstract. An enhanced microscopic void growth-based damage model for the anisotropic ductile metal is introduced in this paper. In this work, for consideration of the anisotropic behavior of sheet metal, the Hill48 quadratic yield criterion is adopted instead of the von Mises yield function. The proposed fracture criterion is formulated by transforming principal stress components into stress triaxiality and Lode parameter space. In addition, the influence of shear damage evolution due to the assumption that the voids are sheared and rotated during deformed configuration is also taken into account. The novel damage model is calibrated via the uniaxial tension tests, the R-notched and shear specimens are specifically designed and simultaneously conducted by both experiments and numerical simulations to validate its predictability of ductile fracture over various stress states.

Keywords: Ductile fracture, Lode parameter, void growth model, R-notched test, fracture strain.

1 Introduction

The ductile fracture phenomenon of metallic material is usually seen in the manufacturing process of formed parts. Nowadays, with the rapid development and popularity of personal computers, the process of product design and failure prediction becomes easier and is a prerequisite in the process design stage. The roots of ductile damage initiation have been proven to be due to microscopic void initiation, growth, and coalescence in the matrix material. Modeling crack initiation in the plastic media is pioneered by McClintock [1]. The firstly proposed crack criteria suggested that plastic failure is governed by stress triaxiality only such as fracture initiates at the locations that have high-stress triaxiality. The several typical damage criteria, which have been acknowledged and widely applied in the fracture mechanics community due to their simplicity in calibrating material parameters, can be mentioned like Oyane et al. [2], Wilkins et al. [3]. Later, ductile fracture investigation was enriched by considering a wide range of stress triaxiality from -1/3 to approximately 1.0 [4]. Accordingly, ductile damage of material under compression, pure shear, uniaxial tension loads take place at the specific values of stress triaxiality, respectively. More recently, the Lode angle dependence on ductile fracture behavior during the loading process was confirmed by Bai

and Wierzbicki [5] and they proposed a three-dimension fracture locus of aluminum alloy AA2024-T351 which was constructed in space of equivalent plastic strain $\bar{\varepsilon}^p$, stress triaxiality η and Lode parameter θ. The clear evidence of Lode parameter dependence on ductile failure is reinforced for a variety of materials such as tubular steel grades [6] and porous plasticity [7] materials. For finding fracture characterization, the experiments are usually conducted for several various sample types that present respective stress states, for example, notched, center hole, shear, plane strain, and biaxial stretching specimens.

Recently, Zhang et al. [8] developed a coupled CDM model using Hill48 yield criterion for predicting alloy sheet Ti-6Al-4V at room temperature. The proposed model allows predicting shear damage including considering Lode angle dependency to ductile damage parameter. It is different from the coupled damage model, uncoupled ones using a damage variable that is independent of the elastoplastic behavior of the material, and crack initiation is considered to occur once the damage parameter reaches a critical value. More recently, Park et al. [9] modified Lou-Huh ductile fracture criterion by replacing the von Mises yield criterion with the Hill48 yield function which is suitable for forming limit diagram prediction of advanced high-strength steel sheets under a large range of stress triaxiality. Although the above-mentioned damage models provide the fracture prediction capabilities of various metallic materials and their alloys. Nevertheless, reliable predictability of the constitutive models is strongly dependent on the mechanical characterizations of each specific material. Therefore, developing a novel damage model to accurately describe ductile fracture behavior is always a fascinating topic in the community of fracture mechanics.

This paper is concerned with modifying a void growth-based fractured prediction criterion for anisotropic sheet metal. A coupled damage model is developed by incorporating a damage variable into yield function Hill48 to consider the anisotropy of the material. For validation purposes, experiments are conducted for aluminum alloy AA5052-H32 to investigate ductile fracture. Particularly, the tensile tests are performed to identify the necessary material parameters of the damage model. Also, the series of tensile tests of R-notched specimens are done in both experiments and numerical simulations in various directions with respect to the rolling direction to validate the applicability of the proposed ductile fracture model in predicting the ductile fracture under different stress states.

2 Ductile Damage Model

2.1 Void Growth Based Ductile Fracture Criterion

A modified McClintock fracture criterion [10] that is based on the growth of ellipsoidal voids in the matrix material is adopted in this work. By using a superposition method of the cylindrical void growth rates proposed by McClintock [1], Dung introduced three damage rates corresponding to three major growth directions of an empty void as follows [10, 11]:

$$dD_a = \left[F_{ol} \times \cosh\left(\frac{\sqrt{3}(1-m)}{4} \frac{\sigma_b - \sigma_c}{\sigma_f} \right) + \frac{3}{4} \frac{\sigma_a - \sigma_b - \sigma_c}{\sigma_f} \right] d\bar{\varepsilon}^p$$

$$dD_b = \left[F_{ol} \times \cosh\left(\frac{\sqrt{3}(1-m)}{4} \frac{\sigma_a - \sigma_c}{\sigma_f} \right) + \frac{3}{4} \frac{\sigma_b - \sigma_a - \sigma_c}{\sigma_f} \right] d\bar{\varepsilon}^p \quad (1)$$

$$dD_c = \left[F_{ol} \times \cosh\left(\frac{\sqrt{3}(1-m)}{4} \frac{\sigma_a - \sigma_b}{\sigma_f} \right) + \frac{3}{4} \frac{\sigma_c - \sigma_a - \sigma_b}{\sigma_f} \right] d\bar{\varepsilon}^p$$

Where $F_{old} = \frac{\sqrt{3}}{(1-m)} \sinh\left(\frac{\sqrt{3}(1-m)}{4} \frac{\sigma_a + \sigma_b + \sigma_c}{\sigma_f} \right)$; dD_a, dD_b and dD_c present damage rates corresponding to three semi-axis directions of a single ellipsoidal void, respectively; σ_a, σ_b and σ_c are principal stress components; σ_f is flow stress of matrix material and $d\bar{\varepsilon}^p$ is equivalent plastic strain rate; m denotes material parameter depending on hardening property of realistic material.

The ductile fracture due to void growth happening once following damage accumulation reaches a certain value as below:

$$D_g = \max(D_a, D_b, D_c) = \max\left(\int_0^{\bar{\varepsilon}_f^p} (dD_a, dD_b, dD_c) \right) = D_g^f \quad (2)$$

Where $\bar{\varepsilon}_f^p$ is the equivalent plastic strain at fracture; D_g^f is ductile fracture constant which depends on the mechanical characterization of the material.

2.2 Proposed Damage Model

The above-mentioned original crack criterion has two key limitations that are not considering the damage mechanism under a range of low-stress triaxialities such as simple and pure shear states and anisotropic properties of the matrix material. Assuming that the elastoplastic behavior of matrix material obeys Hill48 anisotropic criterion, principal stress space $(\sigma_a, \sigma_b, \sigma_c)$ are transformed into Lode parameter, stress triaxiality, and Hill48 equivalent stress space (L_p, η, σ_e) as follows [9] :

$$\sigma_a = \left(\eta + \frac{3 - L_p}{6\sqrt{T}} \right) \sigma_e;\ \sigma_b = \left(\eta + \frac{2L_p}{6\sqrt{T}} \right) \sigma_e;\ \sigma_c = \left(\eta - \frac{3 + L_p}{6\sqrt{T}} \right) \sigma_e \quad (3)$$

Where the mean stress $\sigma_m = (\sigma_a + \sigma_b + \sigma_c)/3$; principal deviatoric stress $s_i = \sigma_i - \sigma_m,\ (i = a,b,c)$; T is a function of Hill48 anisotropic coefficients, Lode parameter, and rotation angle between principal and rolling directions,

$$T = F\left(\frac{1+L_p}{2}\cos^2\theta + \sin^2\theta\right)^2 + G\left(\cos^2\theta + \frac{1+L_p}{2}\sin^2\theta\right)^2 + \left(H\cos^2 2\theta + \frac{N}{2}\sin^2 2\theta\right)\left(\frac{1-L_p}{2}\right)^2 \quad (4)$$

It should be noted that the sheet thickness is considered to be thin relative to its in-plane dimensions so that we assume that the normal direction (ND) coincides with one of the principal stress directions such as the σ_c direction. With this assumption, the rotation angle θ is now referred to as the angle between specimen cut direction and rolling orientation.

The Hill48 equivalent stress function for anisotropic material can be expressed according to Cauchy stress tensor as shown in eq. (5).

$$\sigma_e = \left[H(\sigma_{11}-\sigma_{22})^2 + F(\sigma_{22}-\sigma_{33})^2 + G(\sigma_{33}-\sigma_{11})^2 + 2N\sigma_{12}^2 + 2L\sigma_{23}^2 + 2M\sigma_{31}^2\right]^{1/2} \quad (5)$$

Where H, F, G, N, L, M are anisotropic parameters determined from Lankford coefficients r_0, r_{45}, r_{90}:

$$H = \frac{r_0}{r_0+1};\ F = \frac{r_0}{r_{90}(r_0+1)};\ G = \frac{1}{r_0+1};\ N = \frac{(r_0+r_{90})(1+2r_{45})}{2r_{90}(1+r_0)};\ L = M = \frac{3}{2} \quad (6)$$

With r_0, r_{45}, r_{90} determined from the uniaxial tensile experiments.

If an assumption of the principal stress state $\sigma_a \geq \sigma_b \geq \sigma_c$ is adopted, then Hill48 equivalent stress and Lode parameter can be calculated as follows:

$$\sigma_e = \sqrt{T(\sigma_a - \sigma_c)^2} \ \text{ and } \ L_p = \frac{2\sigma_b - \sigma_a - \sigma_c}{\sigma_a - \sigma_c} \quad (7)$$

Substituting Eqs. (3) into Eqs (1), (2), and (3), the damage rates are re-addressed in the space of (L_p, η, σ_e) as presented by eq.(8).

Observing fracture initiation takes place in a shear band [12], McClintock indicated that the ductile fracture is not only dominated by void growth but also by shearing and rotational voids. The basis on this, the shear strain due to void shear is calculated by eq. (9).

$$dD_a = \left[F_{ne} \times \cosh\left(\frac{\sqrt{3}(1-m)(1+L_p)R_s}{8\sqrt{T}} \right) + \frac{3R_s}{4}\left(\frac{3-L_p}{3\sqrt{T}} - \eta \right) \right] d\bar{\varepsilon}_e^p$$

$$dD_b = \left[F_{ne} \times \cosh\left(\frac{\sqrt{3}(1-m)R_s}{4\sqrt{T}} \right) + \frac{3R_s}{4}\left(\frac{2L_p}{3\sqrt{T}} - \eta \right) \right] d\bar{\varepsilon}_e^p \tag{8}$$

$$dD_c = \left[F_{ne} \times \cosh\left(\frac{\sqrt{3}(1-m)R_s}{4}\left(\frac{1-L_p}{2\sqrt{T}} \right) \right) + \frac{3R_s}{4}\left(\frac{3+L_p}{3\sqrt{T}} + \eta \right) \right] d\bar{\varepsilon}_e^p$$

Where $F_{new} = \dfrac{\sqrt{3}}{(1-m)} \sinh\left(\dfrac{3\sqrt{3}(1-m)\eta R_s}{4} \right)$; $R_s = \sigma_e / \sigma_f$ denotes the ratio of the equivalent stress to flow stress of matrix material.

$$\varepsilon_s = \ln\left(\frac{\ell}{2r} \right) = \ln\left(\frac{\ell_0}{2r_0} \right) - \frac{1}{D_g^f} \int dD_i, \qquad i = a,b,c \tag{9}$$

Where ℓ_0 and r_0 is the initial distance between two adjacent voids and the initial hole radius, respectively.

Xue [13] proposed an artificial strain to account for void-by-void interaction

$$\varepsilon_{art} = \ln\sqrt{1+\gamma^2} = \ln\sqrt{1+2N\left(\bar{\varepsilon}^p\right)^2} \tag{10}$$

And now, for current work a shear damage variable D_s defined as below,

$$D_s = \frac{\varepsilon_{art}}{\varepsilon_s} = \frac{\ln\sqrt{1+2N\left(\bar{\varepsilon}^p\right)^2}}{\ln\left(\dfrac{\ell_0}{2r_0} \right) - \dfrac{1}{D_g^f}\int dD_i} \tag{11}$$

Damage indicator is proposed to take into account for general loading case written as follows,

$$D_t = D_g + g(\theta) D_s \tag{12}$$

Here $g(\theta) = 1 - \mathrm{abs}(\theta)$ is a weighting function recommended by Trung et al [14] to distinguish axisymmetric and plane strain states.

A coupled ductile failure model is formulated within the context of the local approach to fracture by eq. (13), mechanical deterioration of the matrix material is modeled via ductile damage function $g(D) = 1 - D_t^\beta$ in which D_t presents damage variable as shown in eq. (12) and β denotes softening exponent.

$$\Phi = \sigma_e - g(D)\sigma_f = 0 \tag{13}$$

The proposed damage model (eq. (13)) is implemented via a user material subroutine (UMAT) based on a numerical integration algorithm named the "cutting plane" [15]. UMAT subroutine is then integrated with a finite element program, e.g., ABAQUS software.

3 Experimental Works and Identification of Material Parameters

In this work, the specimens are taken from an AA5052-H32 aluminum alloy sheet of 1.5 mm thickness. The samples are completed by the precisely machined service and all tests are conducted using a universal testing machine with the same pulling speed of 0.5 mm/s. The geometric dimensions of the specimen are given in **Fig. 1**.

The dog-bone specimens are used for testing following ASTM-E8 standard and then used for identifying plasticity flow rule parameters. The true stress-strain curve in this work is assumed to obey Swift hardening law and the values of material constants as shown in **Table 1**. Also, the Lankford coefficients r_0, r_{45}, r_{90} which are used to calculate the anisotropic parameters of the Hill48 yield function are determined following the ASTM-E517 standard as provided in By applying the above-mentioned calculation procedures the critical damage parameter for the proposed failure model are summarized in **Table 3**.

Table 2. The tensile tests of R-notched and shear specimens are used to valid damage model for predicting anisotropic ductile facture at 0-degree, 45-degree and 90-degree directions.

The proposed damage model can only be applied to predict fracture initiation once the following parameters are identified: critical damage variable value due to void growth D_g^f, softening exponent β, and factor relating to the initial void shape $\ell_0 / 2r_0$. In this study, a constant value β of 2.0 is fixed while the parameter D_g^f is identified by comparing the force-displacement curves from experiments and numerical simulations. This is achieved by optimizing an objective function as below:

$$F_{obj} = \sum_{i=1}^{Nu} \left(F_{\exp} - F_{sim} \right)^2 \tag{14}$$

Where $F_{\exp}$ and F_{sim} are the force values obtained from the experiments and numerical simulations, respectively, N_u is the number of discrete data points of force-displacement curves.

Table 1. Material constants of AA5052-H32 aluminum alloy sheet

	E (GPa)	v	K (MPa)	ε_0	n
0 deg.	69	0.32	360.59	0.0050	0.1418
45 deg.	69	0.32	348.28	0.0074	0.1400
90 deg.	69	0.32	355.90	0.0071	0.1445

By applying the above-mentioned calculation procedures the critical damage parameter for the proposed failure model are summarized in **Table 3**.

Table 2. Anisotropic coefficients of Hill48 yield criterion

Lankford coefficients			Anisotropic parameters					
r_0	r_{45}	r_{90}	H	F	G	N	L	M
0.84	0.64	1.51	0.46	0.30	0.54	0.96	1.5	1.5

Table 3. Calibrated damage variable of fracture model

	0-deg.	45-deg.	90-deg.
D_g^f	1.25	1.42	2.25

The ratio $\ell_0 / 2r_0$ is calculated through the initial void volume fraction f_0. i.e.,

$$f_0 = \frac{V_0^{void}}{V_0^{total}} = \frac{4\pi r_0^3}{3\ell_0^3} \text{ which can deduce that } \frac{\ell_0}{2r_0} = \frac{1}{2}\sqrt[3]{\frac{4\pi}{3f_0}} \tag{15}$$

Where V_0^{void} stands for initial single void volume and V_0^{total} denotes the initial volume of a representative volume element containing a single void. The initial void volume fraction can be determined by analyzing the microstructural features of realistic material. In this work, nevertheless, a value f_0 of 0.005 is referred from the literature [16].

4 Prediction of Ductile Fracture

Due to the plasticity anisotropy that exists during the loading process, the fully 3D finite element models are adopted for modeling all specimens. The specimens are meshed using 3D eight-node hexahedral solid elements together with an approximate mesh size of 0.5 mm at the interested zone, where the fracture is expected to occur, is adopted as shown in **Fig. 1**. Also, a coarse-to-fine meshing strategy at the transitive region is used to avoid mesh distortion and to save computational time. The fixed boundary condition is applied to one end of the specimen while the other end of the specimen is applied tensile displacement load. A gauge length of 50 mm which depicts the experimental condition is used to measure the displacement value of each test.

Fig. 2 presents a comparison of load-displacement curves between experiments with those of numerical simulations at 0-degree, 45-degree, and 90-degree directions for the R-notched (R20, R5, R1.5) and shear (SH) specimens. In all of the cases, fracture

displacement value in 90-degree direction is always larger than the other two directions which refects the ductility of current aluminum alloy in transverse orientation is largest. For the R-notched specimens, fracture displacement is smaller when the decrease of notch radius. **Fig. 2** also shows that the maximum tensile force in the 0-degree direction of DB, R20, and R5 specimens is larger compared with that of the two remaining directions. While the overestimation of the tensile force in 90-degree is recorded in R1.5 and SH specimens. From the comparison, it can be observed that the developed damage model gives accurate predictions on the anisotropic plastic deformation behavior while fracture displacement predictions give an acceptable precision. The percentage error of fracture displacement between experimentally measured values and numerical simulation values is calculated by the formula $Err(\%) = \left(\left| u_f^{\exp} - u_f^{sim} \right| / u_f^{\exp} \right) \times 100$ and given in **Table 4**. Where, $u_f^{\exp}$ and u_f^{sim} stand for the fracture displacement in tensile tests obtained by experiments and simulations, respectively.

Fracture initiation at the center of the specimen for R20 and R5 notch specimens is recorded while fracture initiates at the periphery for R1.5 notch and SH specimens regardless of the material orientation. Crack is then propagating along the minimum section which is consistent with the experimental observations as demonstrated in **Fig. 3**.

Table 4. The percentage error of predicting fracture displacement using the damage model.

	DB (%)	R20 (%)	R5 (%)	R1.5 (%)	SH (%)
0 deg.	1.45	0.28	8.51	16.71	13.51
45 deg.	1.88	4.09	6.65	3.95	7.61
90 deg.	0.29	3.26	12.62	5.61	3.05

Fig. 4a presents the stress states on the Lode parameter and stress triaxiality plane. Since the Lode parameter and stress triaxiality obtained from numerical simulations are generally not constant during the entire deformed configuration, their average values are calculated by the following integrals,

$$\bar{L} = \frac{1}{\bar{\varepsilon}_f^p\left(L_p,\eta\right)} \int_0^{\bar{\varepsilon}_f^p} L_p\left(\bar{\varepsilon}^p\right) d\bar{\varepsilon}^p \quad \text{and} \quad \bar{\eta} = \frac{1}{\bar{\varepsilon}_f^p\left(L_P,\eta\right)} \int_0^{\bar{\varepsilon}_f^p} \eta\left(\bar{\varepsilon}^p\right) d\bar{\varepsilon}^p \tag{16}$$

According to Bai and Wierzbicki [5], if a stress state is assumed to be under plane stress, i.e., $\sigma_3 = 0$, this condition uniquely relates the parameters L_p and η given by a cubic function as follow,

$$L_p = -\frac{27}{2}\eta\left(\eta^2 - \frac{1}{3}\right) \tag{17}$$

Using the equation (17), a conceptual representation of stress state in two-dimensional space of the Lode parameter and stress triaxiality is shown by the solid line in **Fig. 4**a. Also, using the equations (16), the stress states obtained from tensile tests of R-notched

and SH specimens in three directions at 0-degree, 45-degree, and 90-degree are presented by circle, square, and triangle symbols, respectively. Noting that the data is extracted from the earliest damage element, i.e., the element at the center of R20 and R5 notch specimens is picked up while the element at free-edge of R1.5 and SH specimens is adopted. As shown in **Fig. 4**a, the R5 specimen presents the plane strain state while the R1.5 specimen gives a stress state in the vicinity of the equibiaxial tension. The state of stress in the middle zone of the equibiaxial tension and plane strain is provided by the R20 specimen while the SH specimen provides the stress state close to simple shear which is defined by the coordinates (L_p, η) = (0.178, 0.168), (0.185, 0.186) and (0.181, 0.219) corresponding to 0-degree, 45-degree, and 90-degree directions, respectively.

It is shown that stress triaxiality plays an important role in governing the ductile fracture initiation such as ductile failure is usually occurring at the highest triaxiality location. In addition, it is also known that when the Lode parameter increases to the value of 0, the fracture strain value increases, whereas it decreases again once we increase further Lode parameter toward the value of 1 [17]. In this work, the failure loci in terms of equivalent plastic strain at fracture are approximated by the exponential function of stress triaxiality, $\bar{\varepsilon}_f^p = a\exp(-b\eta)$, as shown in **Fig. 4**b and approximated by the parabolic function of the Lode parameter, $\bar{\varepsilon}_f^p = cL_p^2 + dL_p + e$, as shown in **Fig. 4**c. In which, a, b, c, d and e are fitted constants and given in **Table 5**. The results show that the plastic fracture locus in the 90-degree direction is higher than that of the other two directions which reflects formability in the transverse direction (90-degree) is better than that present in longitudinal (0-degree) and diagonal (45-degree) directions.

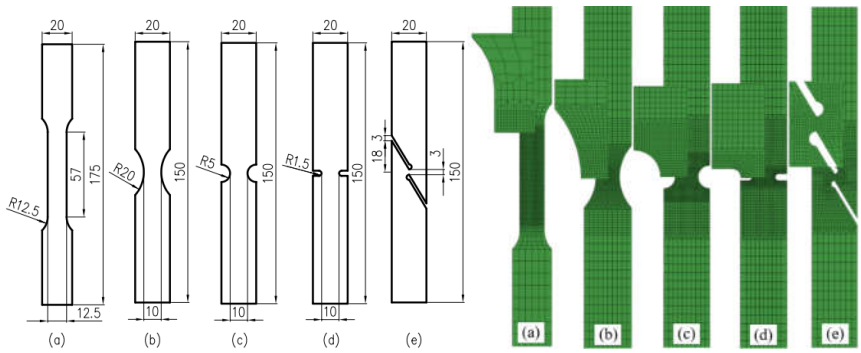

Fig. 1. Dimensions, geormetries and mesh generation of specimens: (a) DB, (b) R20, (c) R5, (d) R1.5 and (d) SH specimens.

Table 5. Fitting parameter values of ductile fracture loci

	a	*b*	*c*	*d*	*e*
0 deg.	0.644	0.677	0.446	0.314	0.445
45 deg.	0.686	0.651	0.568	0.418	0.476
90 deg.	0.890	0.517	0.560	0.421	0.650

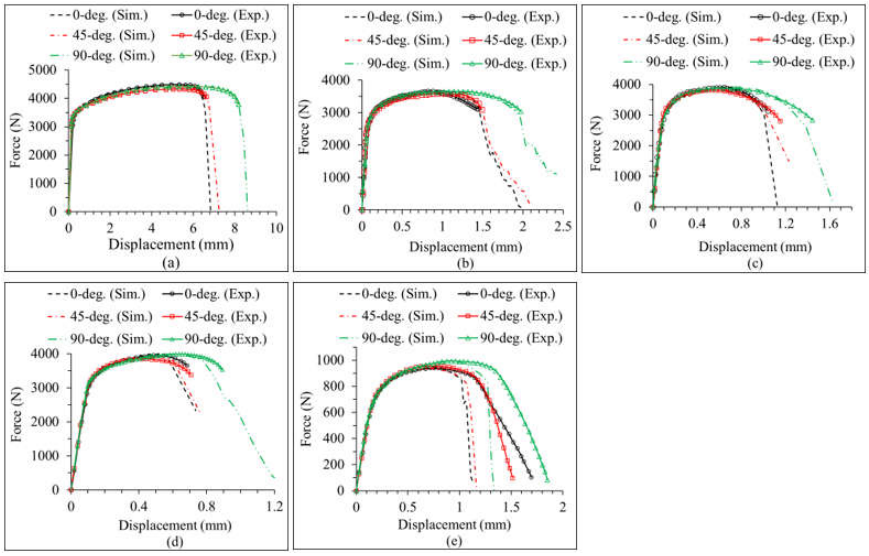

Fig. 2. Force – displacement responses of the different specimens under tensile test in three directions 0-degree, 45-degree and 90-degree with respect to rolling direction (a) dog-bone (DB), (b) R20, (c) R5, (d) R1.5 and shear (SH) specimens.

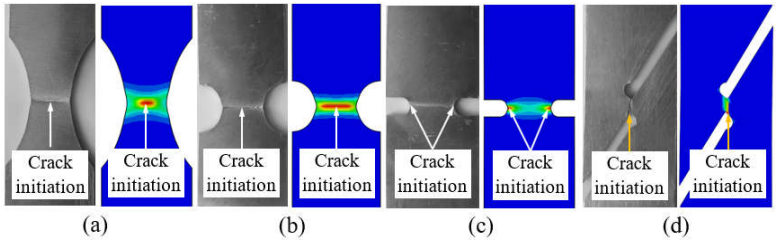

Fig. 3. Crack initiation and path of the specimen by experiments and numerical simulations (the same for all directions): (a) R20, (b) R5, (c) R1.5 and (d) SH specimens

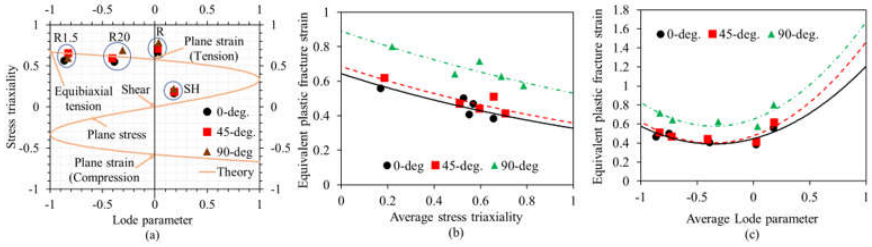

Fig. 4. (a) Presentation of the stress states on the Lode parameter and stress triaxiality plane; The variation of the failure strain as a function of (b) stress triaxiality and (c) Lode parameter

5 Conclusions

In this work, the void growth-based damage model was proposed for predicting ductile fracture initiation of anisotropic sheet metal materials. The developed damage model is applied to predict the ductile fracture behavior of the anisotropic aluminum alloy sheet AA5052-H32 at 0-degree, 45-degree and 90-degree directions. The conclusions can be drawn as follows:

- The tensile tests are performed for several R-notch and shear specimens in order to predict ductile failure initiation under different stress states. The fracture initiation location and the crack path of the R notch and shear specimens are observed to be the same in all three material orientations at 0-degree, 45-degree and 90-degree directions.
- The predictability of the proposed damage model provides an acceptable accuracy with the largest error value of 16.71% for the R1.5 notch specimen at the 0-degree direction.
- The equivalent ductile fracture strain at the 90-degree direction is higher than that of the two remaining directions, and the equivalent ductile fracture strain increases with the decrease of the notch radius. In addition, the plastic strain at fracture of the shear specimens is always largest in all three directions.
- The dependence of ductile fracture strain on stress triaxiality and the Lode parameter was derived as the exponential and parabolic functions, respectively. Moreover, the fractured locus in the 90-degree direction always sits above the other two directions.

Acknowledgment

We acknowledge the support of time and facilities from Ho Chi Minh City University of Technology (HCMUT), VNU-HCM for this study.

References

[1] F. A. McClintock, "A Criterion for Ductile Fracture by the Growth of Holes," *Journal of Applied Mechanics,* vol. 35, no. 2, pp. 363-371, 1968.

[2] M. Oyane, T. Sato, K. Okimoto, and S. Shima, "Criteria for ductile fracture and their applications," *Journal of Mechanical Working Technology,* vol. 4, no. 1, pp. 65-81, 1980.

[3] M. Wilkins, R. Streit, and J. Reaugh, "Cumulative-strain-damage model of ductile fracture: simulation and prediction of engineering fracture tests," Lawrence Livermore National Lab., CA (USA); Science Applications, Inc., San …1980.

[4] Y. Bao and T. Wierzbicki, "On fracture locus in the equivalent strain and stress triaxiality space," *International Journal of Mechanical Sciences,* vol. 46, no. 1, pp. 81-98, 2004.

[5] Y. Bai and T. Wierzbicki, "A new model of metal plasticity and fracture with pressure and Lode dependence," *International journal of plasticity,* vol. 24, no. 6, pp. 1071-1096, 2008.

[6] I. Barsoum and M. Al-Khaled, "The Sensitivity to the Lode Parameter in Ductile Failure of Tubular Steel Grades," *Journal of Pressure Vessel Technology,* vol. 140, no. 3, 2018.

[7] M. Torki, S. Keralavarma, and A. Benzerga, "An analysis of Lode effects in ductile failure," *Journal of the Mechanics and Physics of Solids,* vol. 153, p. 104468, 2021.

[8] K. Zhang, H. Badreddine, and K. Saanouni, "Ductile fracture prediction using enhanced CDM model with Lode angle-dependency for titanium alloy Ti-6Al-4V at room temperature," *Journal of Materials Processing Technology,* vol. 277, p. 116462, 2020.

[9] N. Park, H. Huh, S. J. Lim, Y. Lou, Y. S. Kang, and M. H. Seo, "Fracture-based forming limit criteria for anisotropic materials in sheet metal forming," *International journal of plasticity,* vol. 96, pp. 1-35, 2017.

[10] N. L. Dung, "Three Dimensional Void Growth in Plastic Materials," *Mechanics Research Comunications,* vol. 19, no. 3, p. 227, 1992.

[11] N. L. Dung, "Plasticity theory of ductile fracture by void growth and coalescence," *Forschung im Ingenieurwesen,* vol. 58, no. 5, pp. 135-140, 1992.

[12] F. A. McClintock, S. M. Kaplan, and C. A. Berg, "Ductile fracture by hole growth in shear bands," *International Journal of Fracture,* vol. 2, no. 4, pp. 614-627, 1966.

[13] L. Xue, "Constitutive modeling of void shearing effect in ductile fracture of porous materials," *Engineering Fracture Mechanics,* vol. 75, no. 11, pp. 3343-3366, 7// 2008.

[14] N. T. Nguyen, D. Y. Kim, and H. Y. Kim, "A continuous damage fracture model to predict formability of sheet metal," *Fatigue & Fracture of Engineering Materials & Structures,* vol. 36, no. 3, pp. 202-216, 2013.

[15] M. Ortiz and J. Simo, "An analysis of a new class of integration algorithms for elastoplastic constitutive relations," *International Journal for Numerical Methods in Engineering,* vol. 23, no. 3, pp. 353-366, 1986.

[16] H. H. Nguyen and H. C. Vu, "Forming Limit Prediction of Anisotropic Aluminum Magnesium Alloy Sheet AA5052-H32 Using Micromechanical Damage Model," *Journal of Materials Engineering and Performance,* vol. 29, no. 7, pp. 4677-4691, 2020/07/01 2020.

[17] K. Danas and P. Ponte Castañeda, "Influence of the Lode parameter and the stress triaxiality on the failure of elasto-plastic porous materials," *International Journal of Solids and Structures,* vol. 49, no. 11, pp. 1325-1342, 2012/06/01/ 2012.